



# An Experimental Study of Underwater Acoustic Channel Impulse Response Distributions in a River

Li Wei, Cheng Fan, Zhaohui Wang

Michigan Technological University

Houghton, Michigan, USA

liwei@mtu.edu, fancheng@mtu.edu, zhaohuiw@mtu.edu

## ABSTRACT

In this paper, we present an analysis of the distributions of the underwater acoustic (UWA) channel impulse response (CIR) under various weather conditions. Three field nodes were deployed across a shallow river in three different seasons. The UWA CIRs were estimated from the received OFDM waveform, which had been intensively transmitted three times per minute during three deployments. A weather station monitored the environmental data every 5 minutes during the experiment. The distribution of the tap gain and delay spreads of CIR samples under various weather conditions were estimated with 4 classic distributions. The CIRs variations affected by the temperature, solar radiation, wind speed, and precipitation rate are illustrated in case studies.

## CCS CONCEPTS

• **General and reference** → **General conference proceedings.**

## KEYWORDS

Underwater acoustic communication, field experiment system, channel impulse response

### ACM Reference Format:

Li Wei, Cheng Fan, Zhaohui Wang. 2022. An Experimental Study of Underwater Acoustic Channel Impulse Response Distributions in a River. In *The 16th International Conference on Underwater Networks & Systems (WUWNet'22)*, November 14–16, 2022, Boston, MA, USA. ACM, New York, NY, USA, 8 pages. <https://doi.org/10.1145/3567600.3568155>

## 1 INTRODUCTION

There are a variety of novel underwater infrastructures that have recently emerged, such as offshore wind generators, deep-sea aquaculture facilities, underwater data center systems, offshore drilling platforms with the subsea oil tree, etc. The rapid growth of underwater mobile systems is employed for the construction, deployment, inspection, and maintenance of these underwater infrastructures. The underwater wireless communication and networking system plays an increasingly important part in controlling, coordinating, and cooperating with these underwater mobile systems. Due to the physical characteristics of water as the wireless communication media, radio-frequency (RF) electrical-magnetic waveform can only

propagate an extremely limited distance in the underwater environment, as well as the magnetic inductive waveform and optical waveform. The underwater acoustic (UWA) communication, which has a balanced power efficiency and data rate performance, is the only practical paradigm for kilometer-range underwater wireless communications.

Due to the distinctive physical characteristics of sound propagation in water, the UWA channel is considered one of the most challenging wireless communication channels that are different from the well-studied and standardized terrestrial RF channels [8–10, 16]. The UWA channel usually have spatial-temporal correlated characteristics [1, 7, 9, 11]. Besides the movement of the transmitters and receivers, most of the environmental factors influencing the UWA channel characteristics are mainly related to variations from two perspectives, namely the sound interactions with the surface or bottom and the inhomogeneity of the water medium [20]. The localized geographic features, such as the topography of the bottom and components of sediment, strongly affect the sound ray tracing spreading patterns from the bottom reflection perspective. In addition, temporal variational factors, such as the weather conditions and the hydrodynamic movements of the water body, affect the UWA channel characteristics by agitating the surface reflections and fluctuating the inhomogeneity of the water medium physical properties, namely salinity/conductivity (C), temperature (T) and pressure/depth (D). These spatial and/or temporal variational factors result in UWA channels observed in different field experiments often follow distinct patterns [9].

From a communication perspective, all the spatial-temporal variations can be distinguished as two types based on their duration, namely large-scale and small-scale variations [7]. The large-scale variations, which span multiple communication transactions, were considered caused by uncertainties that affect the acoustic link geometry [7]. On the other hand, the small-scale variations, which occur over a single communication transaction, are considered a consequence of scattering and instantaneous motion [7]. Studying the small-scale variations is meaningful for the analysis of signal processing algorithms and network protocol designs, while studying the large-scale variations can benefit the analysis of strategic system configurations, such as the transmitting power level configuration, as well as the assessment of outage probabilities and statistical coverage for using a particular modulation mode and network protocol configuration.

Much research has been carried out on using machine learning for adaptive UWA communication in recent years [2–4, 13]. In an ideal case, a large amount of UWA channel impulse response (CIR) data for training and evaluating these machine learning models should be generated by UWA channel simulators. However, existing



This work is licensed under a [Creative Commons Attribution International 4.0 License](https://creativecommons.org/licenses/by/4.0/).

WUWNet'22, November 14–16, 2022, Boston, MA, USA

© 2022 Copyright held by the owner/author(s).

ACM ISBN 978-1-4503-9952-4/22/11.

<https://doi.org/10.1145/3567600.3568155>

UWA channel simulators can usually only simulate certain aspects of the channel. A few UWA channel models have demonstrated the capability to simulate the CIRs that match the data on a time scale appropriate for practical adaptive communication scenarios [9, 20]. Even if such a simulator exists, it is difficult to provide sufficient detailed data on environmental factors, especially their temporal variations, for a realistic simulation. Thus, the field experiment data still play an essential part in the analysis and evaluation of UWA communication designs [9, 20]. In [20], a database of ocean CIR was proposed, and the characteristics of interests for the UWA channel were pointed out to ensure the validity and reusability of the UWA channel data for UWA communication performance evaluation purposes. However, besides the CIR data itself, the real-time environmental data, such as the air temperature, wind, rain, etc., can also be utilized for predicting the UWA channel state, thereby contributing to the optimal adaptive UWA communication scheme selection.

Due to the high costs, most existing field experiments transmit waveform either intensively in a burst for short-term tests or periodically once every tens of minutes for long-term tests. The CIRs obtained in either experiment scheduling can usually only reflect small-scale or large-scale variations, but hardly both. In short-term experiments that deploy and recover the equipment during the same voyage, a typical experiment design is to transmit the designed waveform in a burst of several hundreds of packets or data frames, i.e., in [14, 18]. The intensive transmission schedule targets obtaining sufficient data samples to demonstrate the effectiveness of the studied algorithms. Since leaving the equipment in water overnight may not be allowed in the shallow water area or the high costs of ship voyages to offshore areas, intense transmitting scheduling is preferred for minimizing the total deployment time. The short-term intense transmitting scheduling can better help observe small-scale variations due to more CIR samples in a short period being obtained. However, the large-scale variations that span hours or days may not be able to be observed during the short total deployment time. In long-term experiments that recover the deployed equipment in a second voyage, the waveform is usually periodically transmitted in a frequency as low as once every 15-60 minutes, i.e., the SPACE08 and MACE10 experiments in [7] or the KWAUG14 experiment in [11]. The periodical transmission schedule can obtain diverse data samples at different times of the day, and the long idle time between transmissions can extend the total battery lifetime by utilizing the recovery effect of the battery, and transmitting in a burst will drain the battery faster due to the battery rate capacity effect [17]. According to existing field experiment data, neither of these two experiment designs can obtain a decent histogram of the UWA CIRs that can illustrate both the small-scale and large-scale variations, especially for studying the spatial-temporal correlations of UWA CIRs and the environment data.

This paper presents an experimental study of UWA CIR by receiving an intensively transmitted orthogonal frequency division multiplexing (OFDM) waveform with real-time weather information for several days. The CIR data were collected at the exact location but under various weather conditions in different seasons. The temperature, solar radiation, wind speed, and precipitation are observed as the primary weather factors that influence the UWA

channel. The obtained data has been organized as a database consisting of millions of CIR data samples and corresponding real-time weather information at a minute-level sampling rate, which could facilitate future machine learning research of UWA communication. The CIR data at different typical weather conditions are introduced in detail in the case studies.

## 2 EXPERIMENT DESIGN

The objective of the present experiment was to build a database of intensively sampled UWA CIR with the corresponding real-time environmental data. Then, the correlations between weather data and distributions of CIR can be studied.

### 2.1 Hardware System

The hardware system consists of a control center, an RF master node, multiple field nodes, and environmental data sensors, including a weather station and web cameras monitoring the surrounding area. The schematic diagram of the experiment system is shown in Fig. 1.

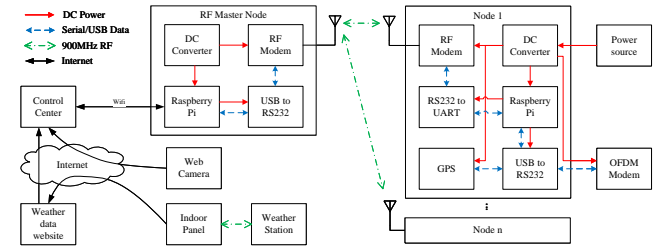
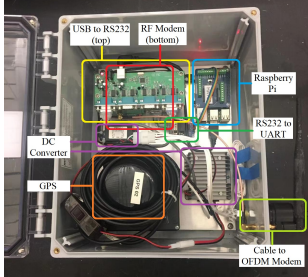


Figure 1: Schematic diagram of the experiment system

The field node employed in this experiment is a low-cost design version of the Ocean-TUNE[17] test-bed surface nodes, which integrate commercial devices. A field node consists of a control box, an AquaSeNT AM-OFDM-13A acoustic modem, and a power source. As shown in Fig. 2, a control box hosts a Raspberry Pi as the host device, a MicroHard n920 RF modem for remote control, a GPS, two different serial port converters, and two DC-DC converters providing 12V and 5V DC power supply. In different situations, the Raspberry Pi can be remotely accessed via the on-board WiFi module, the RF modem connecting to the console port, or the acoustic modem with SeaLinx[5] acoustic remote control module running. The housing of the field node should be both submersible and weatherproof. A sizeable diurnal amplitude can cause condensation to accumulate inside the box, and the accumulated dew may cause short circuits of electronic devices. Since condensation may accumulate inside the housing, waterproof penetration connectors with bulkheads are preferred over cable glands for connecting the control box with other equipment. The box should avoid having clear windows on the top. All the electronic devices should be mounted on an elevated panel, and wires should be appropriately connected and organized. Some desiccant packs could be kept in the box during the deployment time.

Since the RF modems are working in a master-slave mode, an RF master node works as the gateway node connecting the control center and all field nodes. The RF master node was deployed inside the building, which is within the WiFi coverage and can overlook all

field nodes. By remote accessing the Raspberry Pi of the RF master node, one can use a serial port terminal program like Minicom to type commands, operate the master RF modem, and communicate with Raspberry Pis in each field node control box.



**Figure 2: Field node control box**



**Figure 3: Weather station outdoor sensor**

As shown in Fig. 3, the Sainlogic FT0835-plus weather station used in this experiment is a smart home device that costs less than two hundred dollars. The outdoor weather station sensor first reports data samples to an indoor control panel via a 900MHz RF link. Then, the indoor control panel will upload the weather data to a weather data website once every minute. The 5-minute average weather data will be recorded on the website, including historical data from all other available weather stations in the neighborhood. A python crawler script was developed to collect a weather station data sample and a screenshot of the public web camera from corresponding websites every minute.

### 2.2 Transmitted OFDM Waveform

As shown in Fig. 4, the transmitted waveform consists of several preambles, 20 ZP-OFDM data blocks, a 1s idle time for recording the background noise, and an ending Hyperbolic Frequency Modulation (HFM) chirp. The total duration of the waveform is about 9s, but when it is transmitted by the AquaSeNT OFDM modem, an extra preamble will be added to the waveform. If the modem-added preamble is not detected or correctly decoded, the waveform will not be recorded by the receiving modem.

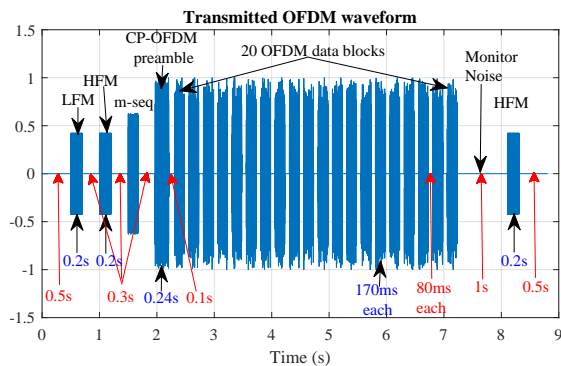


**Figure 4: The transmitted OFDM waveform**

The transmitted waveform uses the 21-27kHz frequency range. For the OFDM data blocks, there are 1024 subcarriers uniformly allocated in the 6kHz bandwidth, which consists of 256 pilot subcarriers, 672 data subcarriers, and 96 null subcarriers. Besides the one pilot subcarrier in every 4 adjacent subcarriers, the lowest and highest 32 subcarriers are filled with null subcarriers. All data subcarriers are located in the middle frequency range, and there is one null subcarrier in every 20 adjacent subcarriers among the data subcarriers. Each data block lasts 170ms and is followed by an 80ms guard time interval.

### 2.3 Experiment Procedure

There was 1 transmitter and 2 receivers during 3 deployments. The deployment locations are shown in Fig. 5. The transmitter was deployed at Node A. The 2 receivers were deployed at Node B and Node C during the first two deployments and then changed to Node C and Node D during the third deployment due to location availability issues. The acoustic modems were deployed at the depths around half of the water depths at their deployment locations.

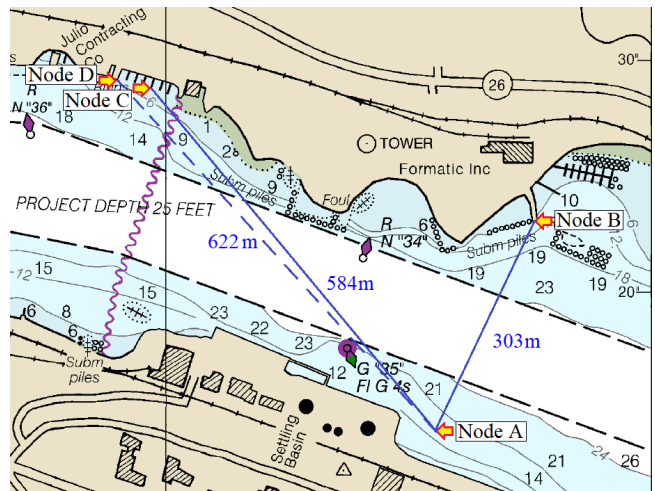


**Figure 5: Deployment locations of the acoustic modems**

The OFDM waveform and a short text message were transmitted during the experiment every 20s. Meanwhile, a weather station mounted at Node A reported the weather data every minute to a weather data website. The website logged the five-minute average of the weather data of all weather stations nearby. The screenshot of the webcam monitoring the experiment area was recorded every 5 minutes, which provides a bird-view of the river surface.

## 3 RESULTS AND ANALYSIS

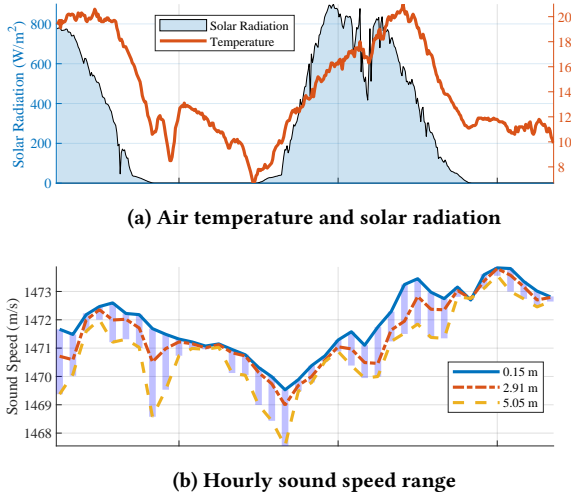
### 3.1 Data obtained

There are three types of data obtained from the presented experiment, namely the environmental data, the communication performance measures obtained from decoding the packet headers, and the channel information from processing the received waveform. All these data are organized with the time and equipment ID information in a MySQL database. The weather data from the weather

**Table 1: Number of transmitted packets and obtained CIR samples**

Start Date	TX waveform	Obtained CIR samples		
		Node B	Node C	Node D
12/24/2021	19788	1555520	1581920	0
04/21/2022	29532	2352960	2358800	0
04/30/2022	1166	93200	77760	0
05/19/2022	10496	0	788560	768640
05/22/2022	26587	0	1793680	1755200

stations include the temperature, dew point, humidity, wind speed, wind gust, pressure, precipitation rate, solar radiation rate, etc. The OFDM modem generated a packet header for each OFDM waveform and text message transmission. By decoding this header, several performance measures were provided in the acoustic modem log file, including input signal-to-noise ratio (INSNR), pilot signal-to-noise ratio (PSNR), effective signal-to-noise ratio [12], center frequency offset (CFO), etc. The received OFDM waveform was stored in the modem only when the packet header had been correctly decoded. There are 4 receiving hydrophones on each acoustic modem, and there are 20 OFDM blocks within each OFDM waveform. Thus, 80 CIR samples can be obtained from a successfully decoded OFDM waveform packet. The total CIR samples obtained during each deployment are listed in Table 1.

**Figure 6: An example of hourly sound speed profile ranges change with air temperature and solar radiation.**

### 3.2 Channel Impulse Response Results and Analysis

The CIRs are estimated with the received signal at the frequencies of pilot subcarriers with both least squares (LS) and SpaRSA estimator [15]. By grouping the CIRs obtained every 15 minutes, here we

briefly reviewed the CIR in the time domain from the arrival time distributions of the multi-paths, as well as the tap gain distributions.

**3.2.1 The Arrival Time of Significant Taps.** After aligning the main peak value with the largest magnitude in a time domain CIR sample to a specific location. A significant tap in a CIR sample is a value whose magnitude is larger than both adjacent values and 0.05 of the largest magnitude value. By histogram of the arrival time of the 10 largest significant taps, the distribution of significant tap arrival times is shown in the first rows in Fig. 12.

**3.2.2 The Tap Gain Distributions.** The histogram of the main peak gain is used to fit the Rayleigh, Rician, Log-Normal, and Nakagami distributions. The parameters of these distributions are estimated by calculating the corresponding observed CIR values in each 15-minute time window. Then, the Jensen–Shannon (JS) divergence [6] of the observed CIR histogram and each distribution with its estimated parameters are calculated. The distribution with the lowest JS divergence value fits the observed CIR histogram the best. The second rows in Fig. 12 showed how the JS divergences vary with time. The color of the shadow on the top part of each figure denotes which distribution has the least JS divergence during each time window.

## 4 CASE STUDY: WATER TEMPERATURE DISTRIBUTION

Since the experiments were in a shallow freshwater area, the water temperature distribution is the main factor that affects the sound speed profile (SSP). With an inhomogeneous distributed SSP, the sound ray will travel along a curved ray. The CIRs observed in the experiment show that the water temperature distribution significantly affected the UWA channel.

### 4.1 UWA Channel affected by temperature and solar radiation

The UWA CIRs at different weather conditions, which lead to different water temperature distributions, are shown in Fig. 11 and Fig. 12. The first row of Fig. 11 show the air temperature and solar radiation data that affect the water temperature. The second row shows the wind speed and precipitation rate that affects the water surface condition. The third row shows the packet loss ratio and the PSNR range of received packet headers for each 15-minute time window. The blue line is the average PSNR, and the light blue shading area denotes the 90% middle-value range PSNR values. The fourth row shows the average and the 90% middle-value range of the bit error rate (BER) of the received OFDM waveform.

The results from two sunny summer days are shown in Fig. 11 (a). It is shown that both the packet loss ratio and BER increase and the PSNR decreases when the solar radiation and temperature decrease due to the sunset. For data during a gloomy summer day shown in Fig. 11 (b) and (c), the variation ranges of temperature and solar radiation rate is smaller, which leads to better UWA communication performances with higher PSNR and lower packet loss ratio and BER. This can be a good train data set for reinforcement learning studies that try to schedule UWA communication at optimal time windows. We measured the SSP at Node A once every 1 hour during a summer day. The sound speed range at different times with

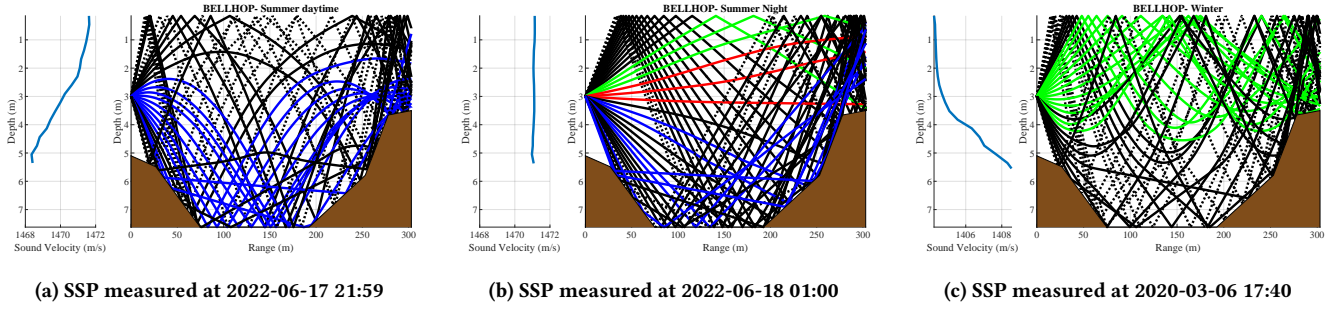


**Figure 7: BELLHOP simulated ray tracing with sound speed profiles measured in field experiments. (Green lines denote rays with surface reflections only, blue lines denote rays with bottom reflections only, red lines denote rays with neither surface nor bottom reflection, and black lines denote rays with both surface and bottom reflections. The solid black lines are rays with no more than 4 reflections, and the dot-dashed black lines are rays with 4 to 6 reflections in total.)**

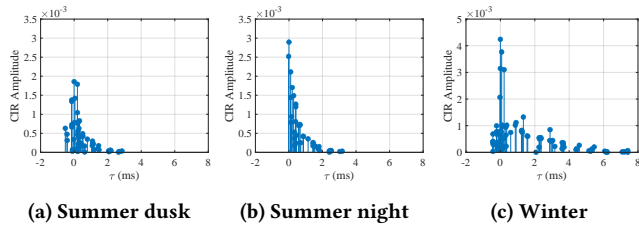


**Figure 8: BELLHOP simulated channel impulse response delay profiles.**

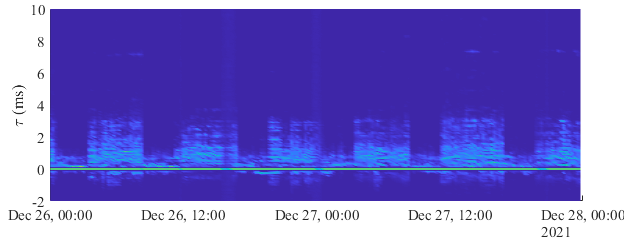


**Figure 9: Significant peak delay distribution at Node B**

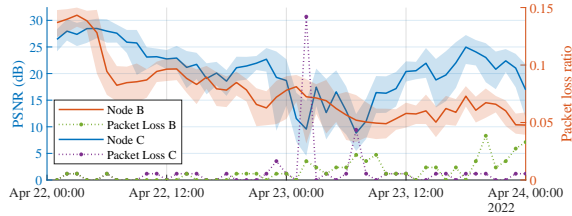


**Figure 10: Packet loss ratio and PSNR during a flood**

corresponding temperature and solar radiation rate is shown in Fig. 6. It shows that the sound speed range is more extensive during dusk, similar to the time ranges when the UWA channel becomes challenging in Fig. 11 (a).

### 4.2 simulation analysis based on historical SSP

We simulated ray tracing of the acoustic wave with the BELLHOP simulator to validate our assumption that the inhomogeneous water temperature distribution leads to different UWA channel conditions in the river.

In Fig. 7, the ray tracing is simulated with the SSP measured near Node A at three different times, namely at the summer dusk, at summer night, and in winter. The water depth in these simulations is similar to the natural environment’s UWA channel between Node A and Node B. With the given water depth and communication distance, the observed temperature differences at summer dusk and winter are significant enough to eliminate the line-of-sight ray between the transmitter and the receiver. When the surface water temperature is higher on sunny summer days, the sound speed is higher at the shallower depth, which leads to the sound rays bending towards the bottom, as shown in Fig. 7 (a). When the surface water temperature is lower in winter, the sound speed is higher at the deeper depth, which leads to the sound rays bending towards the surface, as shown in Fig. 7 (c). With the surface and bottom reflection losses were set to empirical values as 1 and 10, respectively [19], the simulated CIRs of these three cases are shown in Fig. 8. The summer dusk case suffers the most severe attenuation, while the delay spread for the winter case lasts the longest time.

## 5 CASE STUDY: WATER SURFACE CONDITION

The water surface condition can be affected by wind speed and precipitation rate. As shown in Fig. 13 (a) and (b), when the precipitation rate increases, the PSNR decreases while the packet loss ratio and BER increase. Also, the 90% middle-value range of these UWA communication performance-related parameters is wider when the precipitation rate and wind speed are larger.

During the experiment shown in Fig. 13 (c), the water surface was covered with thin ice and snow. Comparing with Fig. 11 (c), the average PSNRs are at a similar level for open water and ice-covered cases, but the 90% middle-value range of the ice-covered case is larger even when the wind speed is lower.

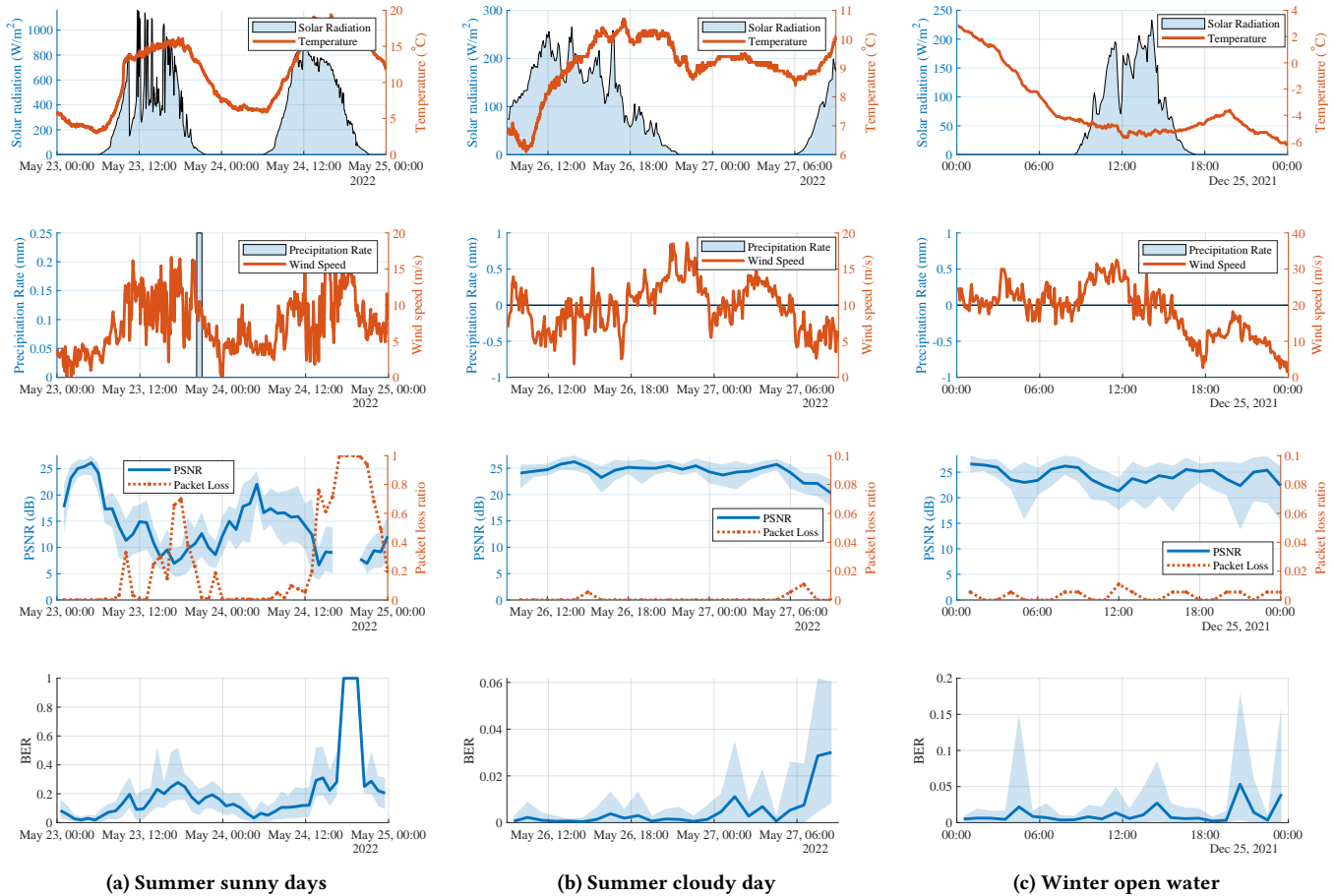


Figure 11: Comparison of SSP affected cases.

## 6 CASE STUDY: NON-WEATHER FACTORS

Other non-weather factors that significantly affect the UWA communication channel could be studied as a pattern.

### 6.1 Ice eater

There was an ice eater near Node B, periodically pumping the bottom water to the surface to keep the dock from freezing. As shown in Fig. 9, the significant peaks converged when the ice eater was turned on.

### 6.2 Flood

There was a flood caused by melt snow around April 23, 2022, which was warned in flood alerts announced by the National Weather Service. As shown in Fig. 10, the PSNR decreased when the flood was developing.

## 7 CONCLUSION

A low-cost field experiment system has been developed to conduct acoustic communication experiments and collect environmental data at a minute-level sampling rate. The proposed system has

been deployed at three different seasons in a year for a UWA communication experiment. An OFDM waveform has been intensely transmitted three times per minute for several days during each deployment under different weather conditions. An ensemble of millions of OFDM waveform blocks has been collected with corresponding weather information, which could benefit the adapting of deep learning models to the UWA communication research.

The temperature profile strongly affects the UWA communication performance since it determines the refraction patterns of the acoustic waveform in the water. The observed daily solar radiation and temperature changes can significantly affect the temperature profile and UWA channel.

The precipitation rate affects both the surface condition and the temperature profile, which lead to the UWA communication performance decreasing and varying in a more extensive range.

## ACKNOWLEDGMENTS

This work was supported by the NSF grant ECCS-1651135 (CA-REER). The authors would like to acknowledge the Great Lakes Research Center of Michigan Technological University for all the support and help during the experiment.

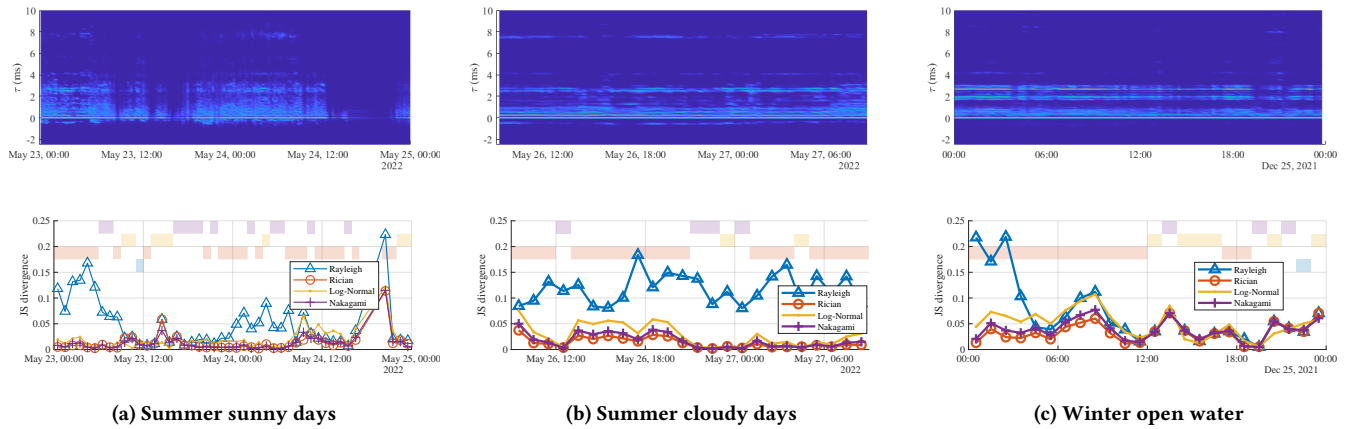


Figure 12: Histogram analysis of water temperature affected UWA CIR at Node C.

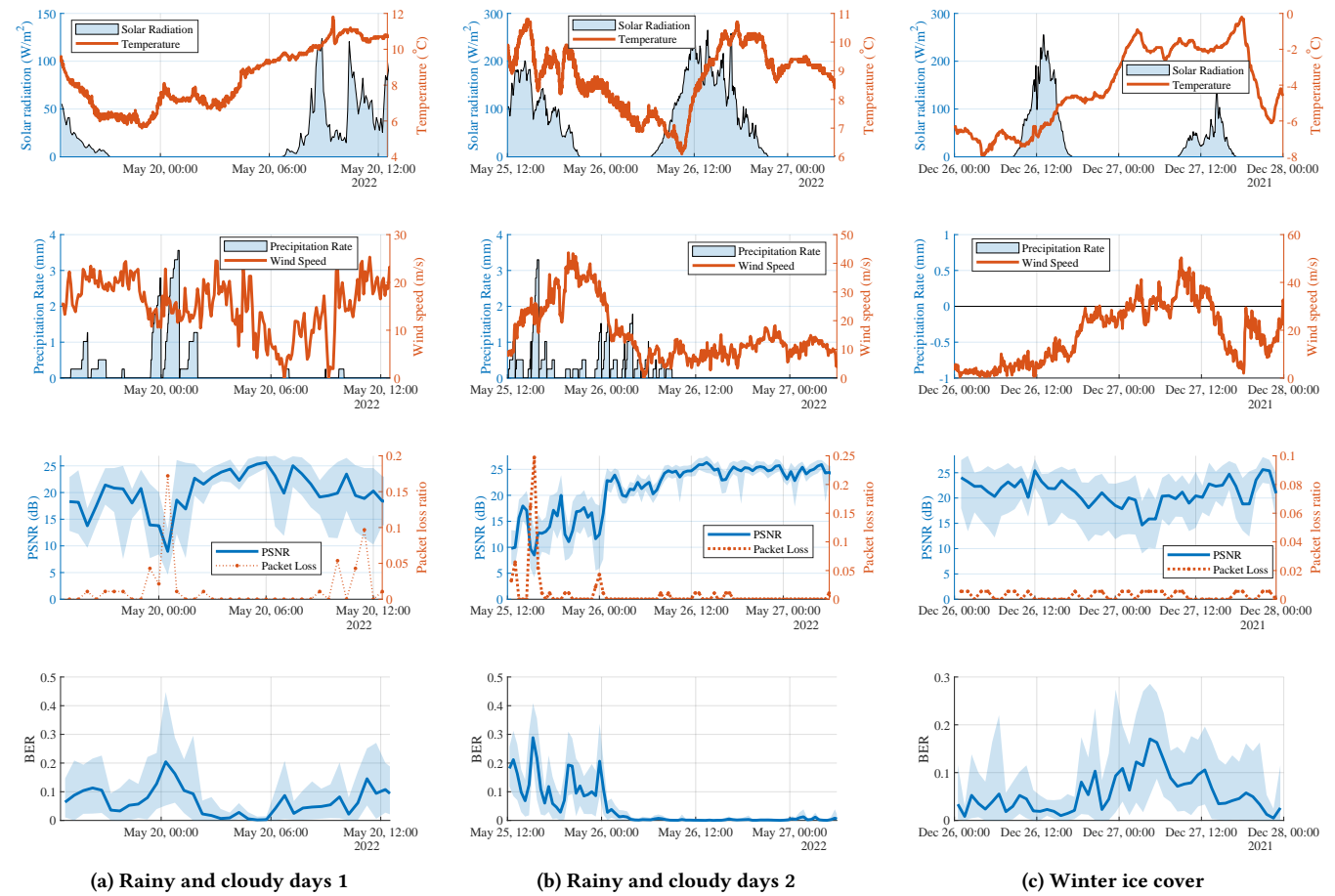


Figure 13: Comparison of surface affected cases.

REFERENCES

[1] Paul C Etter. 2018. *Underwater acoustic modeling and simulation*. CRC press.

[2] Cheng Fan and Zhaohui Wang. 2021. Adaptive Switching for Multimodal Underwater Acoustic Communications Based on Reinforcement Learning. In *The 15th International Conference on Underwater Networks & Systems*. 1–2.

[3] Qiang Fu and Aijun Song. 2018. Adaptive modulation for underwater acoustic communications based on reinforcement learning. In *OCEANS 2018 MTS/IEEE Charleston*. IEEE, 1–8.

- [4] Jianchun Huang and Roe Diamant. 2020. Adaptive modulation for long-range underwater acoustic communication. *IEEE Transactions on Wireless Communications* 19, 10 (2020), 6844–6857.
- [5] Son N Le, Zheng Peng, Jun-Hong Cui, Hao Zhou, and Janny Liao. 2013. Sealinx: A multi-instance protocol stack architecture for underwater networking. In *Proceedings of the Eighth ACM International Conference on Underwater Networks and Systems*. ACM, 46.
- [6] ML Menéndez, JA Pardo, L Pardo, and MC Pardo. 1997. The jensen-shannon divergence. *Journal of the Franklin Institute* 334, 2 (1997), 307–318.
- [7] Parastoo Qarabaqi and Milica Stojanovic. 2013. Statistical characterization and computationally efficient modeling of a class of underwater acoustic communication channels. *IEEE Journal of Oceanic Engineering* 38, 4 (2013), 701–717.
- [8] Andrew C Singer, Jill K Nelson, and Suleyman S Kozat. 2009. Signal processing for underwater acoustic communications. *IEEE Communications Magazine* 47, 1 (2009), 90–96.
- [9] Aijun Song, Milica Stojanovic, and Mandar Chitre. 2019. Editorial Underwater Acoustic Communications: Where We Stand and What Is Next? *IEEE Journal of Oceanic Engineering* 44, 1 (2019), 1–6.
- [10] Milica Stojanovic and James Preisig. 2009. Underwater acoustic communication channels: Propagation models and statistical characterization. *IEEE communications magazine* 47, 1 (2009), 84–89.
- [11] Wensheng Sun and Zhaohui Wang. 2018. Online modeling and prediction of the large-scale temporal variation in underwater acoustic communication channels. *IEEE Access* 6 (2018), 73984–74002.
- [12] Lei Wan, Shiauhe Tsai, and Magnus Almgren. 2006. A fading-insensitive performance metric for a unified link quality model. In *IEEE Wireless Communications and Networking Conference, 2006. WCNC 2006.*, Vol. 4. IEEE, 2110–2114.
- [13] Chaofeng Wang, Zhaohui Wang, Wensheng Sun, and Daniel R Fuhrmann. 2017. Reinforcement learning-based adaptive transmission in time-varying underwater acoustic channels. *IEEE access* 6 (2017), 2541–2558.
- [14] Shuche Wang, Zhiqiang He, Kai Niu, Peng Chen, and Yue Rong. 2020. New results on joint channel and impulsive noise estimation and tracking in underwater acoustic OFDM systems. *IEEE Transactions on Wireless Communications* 19, 4 (2020), 2601–2612.
- [15] Zhaohui Wang, Shengli Zhou, Georgios B Giannakis, Christian R Berger, and Jie Huang. 2011. Frequency-domain oversampling for zero-padded OFDM in underwater acoustic communications. *IEEE Journal of Oceanic Engineering* 37, 1 (2011), 14–24.
- [16] Zhaohui Wang, Shengli Zhou, and Zhengdao Wang. 2018. Underwater distributed antenna systems: Design opportunities and Challenges. *IEEE Communications Magazine* 56, 10 (2018), 178–185.
- [17] Li Wei, Zigeng Wang, Jun Liu, Zheng Peng, and Jun-Hong Cui. 2016. Power efficient deployment planning for wireless oceanographic systems. *IEEE Systems Journal* 12, 1 (2016), 516–526.
- [18] Guang Yang, Qinghua Guo, Hanxue Ding, Qi Yan, and Defeng David Huang. 2021. Joint message-passing-based bidirectional channel estimation and equalization with superimposed training for underwater acoustic communications. *IEEE Journal of Oceanic Engineering* 46, 4 (2021), 1463–1476.
- [19] Kunde Yang, Peng Xiao, Rui Duan, and Yuanliang Ma. 2017. Bayesian inversion for geoacoustic parameters from ocean bottom reflection loss. *Journal of Computational Acoustics* 25, 03 (2017), 1750019.
- [20] T. C. Yang and S. H. Huang. 2016. Building a database of ocean channel impulse responses for underwater acoustic communication performance evaluation: issues, requirements, methods and results. In *Proceedings of the 11th ACM International Conference on Underwater Networks & Systems*. 1–8.